

GPS Solutions

Software Tools for GNSS Interferometric Reflectometry

--Manuscript Draft--

Manuscript Number:			
Full Title:	Software Tools for GNSS Interferometric Reflectometry		
Article Type:	GPS Toolbox		
Keywords:	GPS; GNSS; GNSS-IR; GPS-IR; Multipath; Reflections		
Corresponding Author:	Kristine Marie Larson, PhD University of Colorado Boulder, CO UNITED STATES		
Corresponding Author Secondary Information:			
Corresponding Author's Institution:	University of Colorado		
Corresponding Author's Secondary Institution:			
First Author:	Carolyn Roesler		
First Author Secondary Information:			
Order of Authors:	Carolyn Roesler Kristine Marie Larson, PhD		
Order of Authors Secondary Information:			
Funding Information:	<table border="1" style="width: 100%;"> <tr> <td>National Science Foundation (AGS 1449554)</td> <td>Dr. Kristine Marie Larson</td> </tr> </table>	National Science Foundation (AGS 1449554)	Dr. Kristine Marie Larson
National Science Foundation (AGS 1449554)	Dr. Kristine Marie Larson		
Abstract:	GNSS-R interferometric reflectometry (also known as GNSS-IR, or GPS-IR for GPS signals) is a technique that uses data from geodetic-quality GNSS instruments for sensing the near-field environment. In contrast to positioning, atmospheric, and timing applications of GNSS, GNSS-IR uses signal to noise ratio (SNR) data. Software is provided to translate GNSS files, map GNSS-IR reflection zones, calculate GNSS-IR Nyquist frequencies for varying receiver sample intervals, and estimate changes in the height of a reflecting surface from GNSS SNR data.		

[Click here to view linked References](#)

Software Tools for GNSS Interferometric Reflectometry (GNSS-IR)

Carolyn Roesler and Kristine M. Larson
Department of Aerospace Engineering Sciences
University of Colorado, Boulder
Boulder, CO 80309-0429

Corresponding Author:
Kristine M. Larson
Kristinem.larson@gmail.com
303 492 6583, phone

Abstract

GNSS-R interferometric reflectometry (also known as GNSS-IR, or GPS-IR for GPS signals) is a technique that uses data from geodetic-quality GNSS instruments for sensing the near-field environment. In contrast to positioning, atmospheric, and timing applications of GNSS, GNSS-IR uses signal to noise ratio (SNR) data. Software is provided to translate GNSS files, map GNSS-IR reflection zones, calculate GNSS-IR Nyquist frequencies for varying receiver sample intervals, and estimate changes in the height of a reflecting surface from GNSS SNR data.

Keywords

GPS, GNSS, GPS-IR, GNSS-IR, reflections, multipath

1. Introduction

GNSS-IR is a method for estimating environmental parameters around a geodetic-quality GNSS site. Unlike other reflection techniques, where an antenna is designed to measure reflection signals (Löfgren et al 2011, Camps et al 2015) or a geodetic antenna is rotated to improve its ability to measure reflections (Anderson 2000), GNSS-IR uses data collected with (nominally) multipath-suppressing geodetic-quality GNSS antennas in an upright orientation. GNSS-IR has been demonstrated and validated for measuring surface soil moisture (Larson et al 2008), snow depth (Larson et al 2009; Nievinski and Larson 2014c,d), permafrost melt (Liu and Larson 2018), tides (Larson et al 2013; Löfgren et al 2014; Larson et al 2017), ice-up (Strandberg et al 2017), firm density (Larson et al 2015), and vegetation water content (Wei et al 2015). In addition to these practical demonstrations, Felipe Nievinski developed a simulator that allows a user to test the reflection characteristics for different experimental configurations and surfaces (Nievinski and Larson 2014a,b).

GNSS-IR studies are based on the analysis of SNR patterns created by the interference of direct and reflected (or multipathed) GNSS signals. There is significant literature on the inherent frequencies in GNSS multipath, and we will not repeat it here (e.g. Georgiadou and Kleusberg 1988; Ge et al 2000; Ray and Cannon 2001; Axelrad et al 2005; Bilich and Larson 2007). While the multipath frequencies for a planar reflector change as a satellite rises or sets, Axelrad et al

(2005) proposed a simple change of variable (using $\sin e$ rather than e) that yields one multipath frequency per rising/setting satellite arc. Ignoring the direct signal contribution, SNR data for a single satellite and receiver can be modeled as:

$$SNR(e) = A(e) \sin\left(\frac{4\pi H_R}{\lambda} \sin e + \phi\right) \quad (1)$$

where e is the GNSS satellite elevation angle with respect to the horizon, λ is the GNSS wavelength, ϕ is a phase constant, H_R is the vertical distance between the GNSS antenna phase center and the horizontal reflecting surface, and $A(e)$ represents the amplitude of the SNR data. To be clear, this representation of SNR data is time dependent because e is a function of time. A fuller discussion of the contributions to $A(e)$ can be found in Nievinski and Larson (2014a,c).

When H_R is fixed, surface soil moisture can be derived from the estimated changes in ϕ (Larson et al 2008; Chew et al 2016). Using similar assumptions, A can be used to measure vegetation water content (Wei et al 2015). Changes in A are also important for applications such as sea ice detection (Strandberg et al 2017). In this short note we ignore A and ϕ and focus on the inherent multipath frequency, $2H_R/\lambda$. By estimating the multipath frequency, we have a simple way to determine H_R . This has also been called the reflector height (e.g. Larson and Nievinski 2013), although to be clear, it is not a “height” in a geodetic sense. Here we will use H_R so as to limit the confusion with orthometric and ellipsoidal heights. In the next sections we will discuss our software for GNSS-IR frequency relationships. In particular we are providing codes that do the following:

- Translate GNSS data files stored in the RINEX format
- Map GNSS-IR reflection zones
- Calculate the average Nyquist frequency for a GNSS-IR installation
- Estimate dominant frequencies (and thus H_R) from GNSS SNR data

2. Extracting SNR observations needed for GNSS-IR from a RINEX file

Most GNSS networks provide carrier phase and pseudorange data to users in the RINEX format. These dual-frequency ranging observations are then used with high-precision geodetic or surveying softwares with precise ephemerides to compute daily (or more frequent) Cartesian positions. Unfortunately, the parameters needed for GNSS-IR cannot always be easily extracted from the outputs of high-precision geodetic or surveying softwares. Here we provide Fortran 77 code that translates the GPS (and more generally GNSS) observations stored in a RINEX (Gurtner and Estey 2007) file into a format usable for GNSS-IR research. In the first code (RinexSNR), the elevation and azimuth angles of GPS satellites with respect to the local horizon are computed using the GPS navigation message. The latter is also stored in the RINEX format. The times of the observations (in GPS time, seconds of the day) are also extracted and the SNR observations on the L1, L2, and L5 frequencies are saved. The output format is tabular and thus the information can be easily loaded using other programming languages such as Matlab and python. The current version of the code only reads RINEX version 2.11 format and files with no more than 15 observation types. Signals from non-GPS constellations are ignored.

To support GNSS-IR, we have provided a separate piece of Fortran code (RinexSNR_GNSS) that extracts GNSS SNR observations from a RINEX file. The main difference between the codes is that the first code uses real-time navigation messages to compute satellite ephemerides and the second code uses precise ephemerides. By using the community standard for precise ephemerides (the sp3 format), we can easily compute orbits for any GNSS signal. The current constellations supported are GPS, GLONASS, GALILEO, and BEIDOU. Because all GNSS constellations nominally number their satellites the same way, we rename the non-GPS satellites by adding 100 (GLONASS), 200 (GALILEO), or 300 (BEIDOU). Additional instructions are provided in the readme file.

Both Fortran translation codes use the Cartesian station location in the RINEX header to compute the satellite/station elevation angle. If the RINEX file doesn't have station coordinates, the code stops. It is not necessary that the station location in the header be extremely accurate – but we suggest it be within 50 meters of its truth value. Most RINEX files created by geodesists and surveyors have much better station coordinates than this, with the exception of data from the cryosphere. In these cases the archives often use a single station location for all RINEX files for a given site, even though the station is moving rapidly, in some cases as many as hundreds of meters per year. For these users, we allow time-varying receiver coordinates to be read from an external text file. The user should input a Cartesian position at a given epoch and a Cartesian velocity, in meters and meters/year respectively. This option is not necessary for other GNSS-IR sites.

3. GNSS-IR Reflection Zones

The equations for a Fresnel zone near the surface of the Earth are given in the appendix of Larson and Nievinski (2013); we do not repeat those equations here. The sizes of these elliptical sensing zones are directly sensitive to H_R , the satellite elevation angle (e) and the GNSS transmitter wavelength (L1, L2, or L5). The orientation of the Fresnel zone with respect to the GNSS antenna depends on the azimuth angle of the satellite. The Fresnel zones get smaller and closer to the antenna as the elevation angles increase.

We provide two sets of Matlab codes for mapping reflection zones. The first, `mapview_fresnel_toolbox.m`, plots the Fresnel zones for a given GNSS site in a plain “horizontal” map view. Figure 1 shows example Fresnel zones for a GNSS station located in Boulder, Colorado. Two values of H_R are used. Both examples are for the L1 GPS frequency. The second code, `googleEarthFresnel.m`, provides similar information, with an output kml file that can be loaded into Google Earth. Figure 2 shows a screenshot from Google Earth for the Boulder, Colorado example. Figure 3 shows a screenshot for a GNSS site in Alaska. This particular GNSS site is far above sea level, ~68 meters, and the input H_R value used reflects that. Unlike the Colorado example, only lower elevation angles are shown.

Both `mapview_fresnel_toolbox.m` and `googleEarthFresnel.m` need to know the approximate azimuth of the rising and setting satellites for the GNSS station in question. If the user does not know this information, values can be computed using a separate piece of Matlab code: `do_azims.m`. The `googleEarthFresnel.m` code allows the user to either manually set H_R or to use mean sea level as the reflecting surface. If desiring mean sea level, the code uses the ellipsoidal

GNSS station height and the EGM96 geoid correction (Lemoine et al 1998). For more information on Fresnel zones used for GNSS-IR, the reader is directed to Roussel et al (2014) and Nievinski et al (2016).

4. Frequency Extraction from GNSS-IR: Theoretical Discussion

Although a GNSS receiver will track signals at even time intervals, the interval between 2 samplings of $\sin(e(t))$ will be uneven during any given observing window. Furthermore, different satellite tracks will have different sampling intervals, as GNSS satellites that stay low in the sky move more slowly than those that pass higher in the sky (Figure 4). We use the Lomb Scargle Periodogram (hereafter LSP), designed to detect periodic signals with unevenly spaced observations, to extract the spectral content in SNR data (Lomb 1976; Press et al 1992). In order to express the SNR spectral frequencies directly in terms of H in meters, we scale the sampling variable $\sin(e(t))$ by a wavelength factor. The code `lomb.m` computes the normalized periodogram of a sequence of SNR data sampled at $X(t)=2\sin(e(t))/\lambda$, during an arc over a given elevation angle range $[e_{min} e_{max}]$.

A LSP requires the user to provide the highest frequency factor (`hifac`) and an oversampling factor (`ofac`). We have recast these inputs into variables that are more intuitive for a GNSS-IR analyst. Instead of `hifac` and `ofac`, the user chooses the maximum value of H to be calculated and the desired precision, both in meters. Thus the normalized LSP is calculated at the frequencies $H = [0: \text{desired Precision}: \text{maxHeight}]$. These two user inputs are then converted into `hifac` and `ofac` for input to `lomb.m`. More details can be found in the code `get_ofac_hifac.m`.

The spectral grid can be as large and fine as you want at the expense of a longer computation time. A user may want to compute frequencies up to the pseudo-Nyquist limit (see the next section). For a 1-second GPS sampling rate the pseudo-Nyquist limit is ~ 450 meters with $N=1800$ samples collected in a 30 minutes arc. Using a grid precision of 1 cm, the number of frequencies would be $N_f=45,000$. The scaling of the `lomb.m` algorithm, provided in this Tool Box entry, is of the order of $N_f N \sim 10^8$. For a 5-second GPS sampling rate, this value is reduced by 25 but is still quite large. Instead, for snow accumulation, we have prior knowledge of the frequency range from which to expect a spectral peak. For a GNSS antenna initially set at 2-meters, we might select a maximum grid frequency `maxHeight` of 6 meters. Note that faster implementations of the LSP exist if you would like to check all frequencies (Press and Rybicki 1989).

We cannot guarantee that the highest peak corresponds to the best frequency H_R , as in some instances there is a double peak with close amplitudes. And even if you are on the correct peak, the grid spacing is not the true precision of the spectral peak. For instance, the spectral resolution scales inversely to the length W of the GNSS type observing window, where $W = 2(\sin(e_{max}) - \sin(e_{min}))/\lambda$ in units of inverse meters. It is advisable to have at least one cycle of SNR data in your survey window. Significant frequencies below $1/W$ need to be analyzed carefully as they could be low-frequency residuals from an imperfect removal of the direct SNR signal. Finally, the peak estimate from one LSP may not be statistically reliable, but by taking the daily average or median over tens to hundreds of tracks one can increase the quality of the H_R estimate over a region.

For even sampling, any frequency above the Nyquist frequency will be folded back (aliased) into the lower frequencies. With uneven sampling, the Nyquist-like limit, the limit beyond which no further information from the spectral content of the sampled signal can be extracted, can be much larger than the “Average-Nyquist” frequency computed for the same number of data uniformly sampled during the same time span. This makes intuitive sense because when the spacing varies we collect extra information in the space between two even samples and this can remove the aliasing ambiguity (Press et al. 1992; VanderPlas 2017).

In the context of GNSS-IR, the samples in the observing window are structured, i.e. they are not random. Any structure in the sampling interval will be reflected in the LSP of the signal. Qualitatively the LSP patterns can be represented as the convolution between the window spectrum and the spectrum of the true signal. To discuss a Nyquist-like limit we will look at the spectral characteristics of the observing windows. We provide this discussion so that potential GNSS-users will have an understanding of what GNSS time sampling interval to use to appropriately resolve H_R from their SNR data. We use observations from the GNSS station GLS2. Operators of the station set its receiver-sampling rate to 15 seconds. We select three tracks with the same SNR characteristics and use the L2 frequency data (Figure 5d), but with different survey windows in the elevation angle range [5-20] degrees (Figure 5e). The window spectra are computed up to H of 300 meters. (To estimate the form of the window power spectrum, first compute a LSP on a series of unit measurements. You will need to use a modified version of `lomb.m` that sets the mean to be zero and the variance to be 1).

The southeast track has a nearly uniform sampling (Figure 5e). This results in a power spectrum of the window close to regularly narrow spaced spikes with a cadence of 69 meters (Figure 5a). Yet as the frequency H increases, the shape of the peaks changes. The spikes slightly decrease in power and their tail end spreads. As the sampling becomes less uniform the distortion increases. For the most severe case of uneven sampling found at GLS2 (northeast track) the window spectrum becomes noise-like after 250 meters. This window structure is reflected in the LSP of the SNR (Figure 5a,b)

The distance (cadence) between two spikes stays relatively constant. We will use half of this distance as the pseudo-Nyquist frequency. Any single frequency above this limit will be an imperfect version folded back into the lower frequencies, with a spectrum spread distortion depending on the degree of unevenness in the samplings. For moderately uneven to strong uneven sampled noisy data, the interaction of high-frequency noise bands with the convolution window can be complex with an increased spectral background noise level and eventually create spurious high-leveled peaks. The SNR power spectrums for the three tracks in the range [0-6] meters are similar (Figure 5c) because there is no significant high-frequency noise folded back into this region.

We should clarify that with this type of LSP window, when the power of the second spike is less than ~half the power of the zero-frequency peak, one should be able to detect significant spectral peaks beyond this pseudo-Nyquist frequency, and the true Nyquist-like limit is much larger. For further qualitative details on the effect of uneven-sampling and understanding the LSP the reader is referred to VanderPlas (2017).

To conclude, the exact structure of the LSP window will vary with each site, track, elevation angle range, L-band frequency and GPS receiver sampling rate, but the window LSP signature will vary between the 2 extremes mentioned above. This is one reason for the quality of the LSP across sites and tracks, especially in the presence of noise. We can get an approximate order of magnitude pseudo-Nyquist frequency by using the Average-Nyquist frequency, which ranges between 30-50 meters for GLS2, a sampling rate of 15 seconds, and at the L2 frequency (Table1). For a survey window of length W and N observations the Average-Nyquist frequency is $N/2W$.

Table 1. The pseudo-Nyquist and Average-Nyquist frequencies for the three survey windows from Figure 5. The length of the survey window is $W = 2(\sin(e_{max}) - \sin(e_{min})) / \lambda$.

	<i>Sat 27 Southeast</i>	<i>Sat 30 Northeast</i>	<i>Sat 27 Northeast</i>
Pseudo-Nyquist (m)	$69/2 = 34.5$	$71.5/2 = 35.7$	$85.5/2 = 42.7$
Average-Nyquist (m)	$144/2W = 34.5$	$151/2W = 36.2$	$215/2W = 51.5$

Matlab code is provided to allow a user to calculate the median Average-Nyquist frequency. The user provides a receiver sampling interval (in seconds), the station location, GPS frequency, and elevation angle limits. The code simulates rising and setting satellite information for the GNSS site and outputs the median Average-Nyquist frequency

5. GNSS-IR Examples

Finally, we provide Matlab code to compute sample GNSS-IR results (`sample_gnss_ir.m`). SNR data from GNSS stations from Greenland, Antarctica, and the western U.S are provided. The GNSS sites have one thing in common: they were deployed without any thought that they could be used for GNSS-IR. Although we will refer to GNSS, these particular sites only tracked GPS satellites on the L1 and L2 frequencies. Before discussing the output of this code, we will first describe the various steps within it.

I. Because this is a set of tutorial codes, the user is asked to choose a GPS frequency. The L1 GPS signal generated with the C/A code has the advantage that it is almost always available in RINEX files and it is tracked for all satellites. There can be issues with quality, particularly for some receivers; some of these issues are highlighted by Larson and Nievinski (2013). The L2 GPS signal currently has two codes. The public code (L2C) is far superior to L2P for GNSS-IR. Unfortunately L2C is not always tracked at GNSS sites. As of 2016, L2C is available on 18 GPS satellites. For the sample data files we provided, we strongly recommend using L1 or L2C (when available). None of the example GNSS sites in this tutorial tracked L5 signals, but as with L2C, these new data are excellent for GNSS-IR applications (Tabibi et al 2015).

II. Various defaults have been set. As discussed in the previous section, two LSP parameters need to be defined. For the tutorial, LSP precision is set to 5 mm and the maximum H_R allowed is 8 meters. H_R values smaller than 0.4 meters are not allowed, as GNSS-IR breaks down for small values of H_R (Nievinski and Larson, 2014c). For tower applications, users must change the maximum H_R .

III. The code needs to know the rising and setting satellite arcs for each site. Rather than predefine these values, these codes search for all available satellite data within 45-degree azimuth bins. Once the data for a particular satellite in a given azimuth bin are found, the SNR data are converted to linear units (from dB-Hz to volts/volts) and a low-order polynomial is removed. The low-order polynomial represents the direct signal component which is of no interest for GNSS-IR. A LSP is then produced from these “flattened” SNR traces.

IV. After a LSP is computed for a given rising or setting arc, the code must decide whether the peak in the LSP is significant. Here we have used a simple peak/noise ratio test. This is certainly not the only –or the best– way to compute the significance of a peak. The code allows the user to define over which frequencies the noise metric is computed and what ratio between the peak and noise is required. Other quality control metrics that could be used include a simple amplitude minimum value, the number of points (which would depend on the sampling interval), and the elevation angle difference.

V. The tutorial code generates two kinds of output. A list of the significant H_R results are output to a text file. Plots can be automatically generated either as a summary for all azimuths or in separate azimuth bins. This is currently set to 45-degree azimuth bins, however, this can easily be changed by the user.

VI. Figures 4 and 5 give you an overview of the GNSS-IR steps used for GLS2, a GNSS site in Greenland. In contrast to the Fresnel zones in the Boulder, Colorado case (Figure 2), which had a void in the north, there is 360-degree azimuthal coverage at GLS2 (Figure 6). This is typical for polar regions. The colored lines on Figure 6 represent the approximate azimuths of the rising and setting arcs of single satellite at this site (PRN 30). Figure 7 shows the SNR data for PRN 30 in the four geographic quadrants and their corresponding LSP. Note that at this site the quality of the oscillations is poorer at higher elevation angles. The user can restrict the analysis accordingly. The reflection signal at GLS2 below 10 degrees is quite strong, which serves as a reminder to station operators that elevation masks hinder GNSS-IR applications.

VI. `sample_gnss_ir.m` can be run with five sample files. Here we will only show results for two of the sites: P038 and GLS2. Figure 8 shows L2C GNSS-IR results for station P038. This station is located at an airport in New Mexico with little or no terrain relief. We used the “Separate plots by azimuth bin” option. Figure 8 (top) shows SNR data for the satellites that rise and set for azimuth angles between 180 and 225 degrees. Below we show the LSP results. You can see that the peaks of the LSP are very consistent with a horizontal planar surface. Figure 9 shows GNSS-IR results for the site in Greenland, GLS2 using L1 data on May 24, 2013. In this example we opted to show all azimuths together and the code calculates the median of the peak LSP values, which yields a H_R of 2.97 meters. The user can contrast this with data from the previous week (May 19, 2013), which produces a median H_R of 1.09 meters. The large difference in H_R for these cases is due to a field visit by the station operators who raised the antenna height ~1.9 meters (Larson et al 2015). A sample SNR file from Recovery Lake, Antarctica is also provided.

VII. We have not made phase center offset corrections. If combining multiple frequency H_R retrievals, one should adjust the time series accordingly.

Our goal for distributing these codes is to make it easier for you to visually understand what reflected GNSS signals look like in SNR data. You cannot immediately use the codes in an operational sense, but they can easily be modified for that use. The main change you will need is to convert `sample_gnss_ir.m` into a function. Most typically at this stage all plots would be turned off, and this new function would be called with, e.g., station name, year, day of year, frequency (1,2,or 5), elevation angles limits, desired H_R precision, maximum H_R , and azimuth ranges. One reason we think it is useful to start out evaluating SNR data visually is so that you can see which azimuth and elevation angles are generating usable reflection data. The reflection zone mapping software we have provided earlier gives you a way to validate these azimuth and elevation angle choices. While it is certainly possible to automate the azimuth and elevation angle choices, as we did for PBO H₂O (Larson 2016), you will be able to develop a better automation scheme if you start with the raw SNR data. Visually inspecting GNSS-IR periodograms will also encourage you to think about how to decide which LSP retrievals are significant and which are not.

6. Final Remarks

We hope that these codes will provide guidance for new users of GNSS-IR. The technique is particularly straightforward to use in polar regions (Shean et al 2017; Siegfried et al 2017). With excellent azimuthal coverage at the poles and large planar surfaces, several hundred GNSS-IR reflection retrievals can easily be made per day, yielding an extremely robust daily average. If the GNSS antenna pole is set in ice, GNSS-IR and traditional GNSS vertical measurements can be used to simultaneously constrain the density of the firm layer and snow accumulation (Larson et al 2015). Liu and Larson (2018) recently demonstrated that GNSS-IR can also be used to constrain permafrost behavior in the summer.

The GNSS-IR technique is increasingly being used as a tide gauge (Larson et al 2017). The motivation for doing so is primarily its simultaneous ability to measure changes in the water surface and the antenna phase center in a terrestrial reference frame (Santamaría-Gómez and Watson 2017). For the tide gauge application, additional corrections are needed and codes for those corrections are not provided in this Tool Box contribution. First, a correction is needed if the water height changes significantly during a rising or setting satellite arc (Larson et al 2013), i.e. the so-called \dot{H}_R term. Secondly, a refraction correction must be made (Williams and Nievinski 2017). Because the tide gauge application requires subdaily measurements, significant efforts have been made to improve the resolution of a single H_R value. We direct the reader to Strandberg et al (2016), Reinking (2016), and Wang et al (2018) for additional information on these efforts.

As a final note, we encourage GNSS-IR enthusiasts to take advantage of GNSS-IR simulators (e.g. Nievinski and Larson, 2014d, Roussel et al 2014) and the mapping/Nyquist tools provided here to properly design new GNSS-IR sites. At a minimum, one should:

1. track all frequencies
2. track all codes (i.e. L2C, L5)
3. track all constellations
4. remove elevation angle masks.

If there are significant cost issues related to telemetry, one can choose a receiver sampling interval that both limits those costs and allows reflection monitoring. We also encourage those station operators that need to place their GPS antennas on buildings for reasons of safety to consider placing them near the edge of the roof so as to enable reflection science.

Acknowledgements

KL and CR acknowledge their GNSS-IR colleagues: Eric Small, Clara Chew, Felipe Nievinski, Valery Zavorotny, and John Braun. Kevin Choi helped decipher the google Earth maps. At UNAVCO we thank Fran Boler, Karl Feaux, John Galetzka, Dave Maggert, and Jim Normandeau. We thank Kai Borre, Dmitry Savransky and many others for providing open access code. This research is currently supported by NSF programs in Atmospheric Sciences, EarthScope, and Hydrologic Sciences (NSF Grant AGS 1449554); reflectometry research was previously supported by the NASA Earth Surface and Interior program via NNX12AK21G.

References

- Anderson KD (2000), Determination of water level and tides using interferometric observations of GPS signals, *J. Atmos. Oceanic Technol.*, 17:1118–1127.
- Axelrad P, Larson KM, Jones B (2005) Use of the Correct Satellite Repeat Period to Characterize and Reduce Multipath Errors, Institute of Navigation GNSS 18th International Technical Meeting of the Satellite Division, Long Beach, 13-16 September, 2005, 2638-2648.
- Bilich A, Larson KM (2007) Mapping the GPS Multipath Environment Using the Signal-to-Noise Ratio (SNR), *Radio Science*, 42, RS6003, doi:10.1029/2007RS003652.
- Camps A, Rodriguez-Alvarez N, Valencia E, Forte G, Ramos I, Alonso-Arroyo A, Bosch-Lluis X (2013) Land monitoring using GNSS-R techniques: a review of recent advances. In: *2013 IEEE International Geoscience and Remote Sensing Symposium (IGARSS)*, Melbourne, Australia, 4026-4029, doi: IGARSS.2013.6723716.
- Chew CC, Small EE, Larson KM (2016) An Algorithm for Soil Moisture Estimation Using GPS Interferometric Reflectometry for Bare and Vegetated Soil, *GPS Solutions*, 20(3):525-537, doi:10.1007/s10291-015-0462-4.
- Ge L, Han S, Rizos, C (2000) Multipath mitigation of continuous GPS measurements using an adaptive filter, *GPS Solutions* 4(2):19-30.
- Georgiadou Y, Kleusberg A (1988) On carrier signal multipath effects in relative GPS positioning. *Manuscr Geodaet*, 13:172–179.
- Gurtner W, Estey L (2007) RINEX: The receiver independent exchange format version 2.11, accessed at <ftp://igs.org/pub/data/format/rinex211.txt> , accessed on February 22, 2018.
- Larson KM, Gutmann E, Zavorotny VU, Braun JJ, Williams M, Nievinski FG, Can We Measure Snow Depth with GPS Receivers? *Geophys. Res. Lett.*, 36, L17502, doi:10.1029/2009GL039430, 2009.
- Larson KM, Nievinski FG (2013) GPS Snow Sensing: Results from the EarthScope Plate Boundary Observatory, *GPS Solutions*, 17(1):41-52, doi 10.1007/s10291-012-0259-7.
- Larson KM, Ray RD, Nievinski FG, Freymueller JT (2013) The Accidental Tide Gauge: A GPS Reflections Case Study from Kachemak Bay, Alaska, *IEEE GRSL*, 10(5):1200-1204, doi:10.1109/LGRS.2012.2236075.
- Larson KM (2016) GPS Interferometric Reflectometry: Applications to Surface Soil Moisture, Snow Depth, and Vegetation Water Content in the Western United States, *WIREs Water*, 3, 775-787, doi:10.1002/wat2.1167.

- Larson KM, Ray RD, Williams, SDP (2017) A ten year comparison of water levels measured with a geodetic GPS receiver versus a conventional tide gauge, *J. Atmos. Ocean Tech.*, 34(2):295-307, doi:10.1175/JTECH-D-16-0101.1.
- Lemoine, FG, Kenyon SC, Factor JK, Trimmer RG, Pavlis NK, Chinn DS, Cox CM, Klosko SM, Luthcke SB, Torrence MH, Wang YM, Williamson RG, Pavlis EC, Rapp RH, Olson TR (1998) The Development of the Joint NASA GSFC and the National Imagery and Mapping Agency (NIMA) Geopotential Model EGM96. NASA/TP-1998-206861, July 1998.
- Liu L, Larson, KM (2018) Decadal changes of surface elevation over permafrost area estimated using reflected GPS signals, *The Cryosphere*, 12:477-489, doi:10.5194/tc-12-477-2018.
- Löfgren JS, Haas R, Scherneck HG, Bos MS (2011), Three months of local sea level derived from reflected GNSS signals, *Radio Sci.*, 46:RS0C05, doi:[10.1029/2011RS004693](https://doi.org/10.1029/2011RS004693).
- Löfgren JR, Haas R, Scherneck HG (2014), Sea level time series and ocean tide analysis from multipath signals at five GPS sites in different parts of the world, *J. Geodyn.*, Vol. 80, 66–80.
- Lomb NR (1976), Least-squares frequency-Analysis of unequally spaced data, *Astrophys. Space Sci.*, 39(2):447–462.
- Nievinski FG, Larson, KM (2014a) Forward modeling of GPS multipath for near-surface reflectometry and positioning applications, *GPS Solutions*, 18(2):309-322, doi:10.1007/s10291-013-0331-y.
- Nievinski FG, Larson, KM (2014b) An Open Source GPS Multipath Simulator in Matlab/Octave, *GPS Solutions*, 18(3):473-481, doi:10.1007/s10291-014-0370-z.
- Nievinski FG, Larson KM (2014c) Forward and Inverse modeling of GPS multipath for snow depth estimation, part I: formulation and simulations, *IEEE TGRS*, 52(10):6555-6563, doi:10.1109/TGRS.2013.2297681.
- Nievinski FG, Larson KM (2014d) Forward and Inverse modeling of GPS multipath for snow depth estimation, part II: application and validation, *IEEE TGRS*, 52(10):6564-6573, doi:10.1109/TGRS.2013.2297688.
- Nievinski FG, Silva MF, Boniface K, Monico JFG (2016) GPS Diffractive Reflectometry: Footprint of a Coherent Radio Reflection Inferred From the Sensitivity Kernel of Multipath SNR, *IEEE JSTARS*, 9(10):4884-4891.
- Press WH, Rybicki GB (1989), *Fast algorithm for spectral analysis of unevenly sampled data*, *Astrophysical Journal*, Vol. 338, 277-280, doi: 10.1086/167197.
- Press WH, Teukolsky SA, Vetterling WT, Flannery BP (1992) *Numerical Recipes in Fortran 77*, Vol. 1, 2nd Edition, New York, Cambridge University Press, 569-573.
- Ray JK, Cannon ME (2001) Synergy between Global Positioning System code, carrier, and signal-to-noise ratio multipath errors, *J. Guid. Contr. Dyn.* 24:54-63.
- Reinking J (2016) GNSS-SNR water level using global optimization based on interval analysis *J. Geod. Sci.* 6:80-92.
- Roussel N, Frappart F, Ramillien G, Darrozes J, Desjardins C, Gegout P, Pérosanz P, Biancale R (2014) Simulations of direct and reflected wave trajectories for ground-based GNSS-R experiments, *Geosci. Model Dev.*, 7(5):2261–2279.
- Roussel N, Ramillien G, Frappart F, Darrozes J, Gay A, Biancale R, Striebig N, Hanquiez V, Bertin X, Allain A (2015), Sea level monitoring and sea state estimate using a single geodetic receiver, *Remote Sens. Environ.*, 171:261–277.
- Santamaría-Gómez A, Watson C (2017), Remote leveling of tide gauges using GNSS reflectometry: Case study at Spring Bay, Australia, *GPS Solutions*, 21(2):451-459.

- Shean D, Christiansen K, Larson KM, Ligtenberg SRM, Joughin IR, Smith BE, Stevens CM, Bushuk M, Holland DM (2017) GPS-derived estimates of surface mass balance and ocean-induced basal melt for Pine Island Glacier ice shelf, Antarctica, *The Cryosphere*, 11:2655-2674, doi:10.5194/tc-11-2655-2017.
- Siegfried MR, Medley B, Larson KM, Fricker HA, Tulaczyk S (2017) Snow accumulation variability on a west Antarctic ice sheet observed with GPS reflectometry, 2007-2017, *Geophys. Res. Lett.*, 44(15):7808-7816, doi:10.1002/2017GL074039.
- Strandberg J, Hobiger T, Haas R (2017) Coastal Sea Ice Detection Using Ground-Based GNSS-R, *IEEE GRSL*, 14(9):1552-1556, doi: 10.1109/LGRS.2017.2722041
- Strandberg J, Hobiger T, Haas R (2016) Improving GNSS-R sea level determination through inverse modeling of SNR data, *Radio Sci.*, 51:1286–1296, doi:[10.1002/2016RS006057](https://doi.org/10.1002/2016RS006057). 2016.
- Tabibi S, Nievinski FG, van Dam T, Monico G (2015) Assessment of modernized L5 SNR for ground-based multipath reflectometry applications, *Adv. Space Res.* 55(4), doi:10.1016/j.asr.2014.11.019.
- VanderPlas JT (2017) Understanding the Lomb Scargle Periodogram, accessed February 27, 2018, <https://arxiv.org/pdf/1703.09824.pdf>
- Wang X, Zhang Q, Zhang S (2018) Water levels measured with SNR using wavelet decomposition and and Lomb-Scargle periodogram, *GPS Solutions*, 22:22, <https://doi.org/10.1007/s10291-017-0684-8>.
- Wei W, Larson KM, Small EE, Chew CC, Braun JJ (2015) Using GPS Receivers to Measure Vegetation Water Content, *GPS Solutions*, 19(2):237-248, doi:10.1007/s10291-014-0383-7.
- Williams SDP, Nievinski FG (2017), Tropospheric delays in ground- based GNSS multipath reflectometry-Experimental evidence from coastal sites, *J. Geophys. Res.*,122:2310–2327, doi:10.1002/2016JB013612.

Author Biographies

Dr. Carolyn Roesler received her PhD in aerospace engineering sciences from the University of Colorado in 2014. She is currently a research associate at the University of Colorado.

Dr. Kristine M. Larson received her AB degree in engineering sciences from Harvard University in 1985 and her PhD in geophysics from Scripps Institution of Oceanography, UCSD in 1990. She is a professor in the Department of Aerospace Engineering Sciences at the University of Colorado. Her research focuses on developing new geoscience applications for GPS measurements.

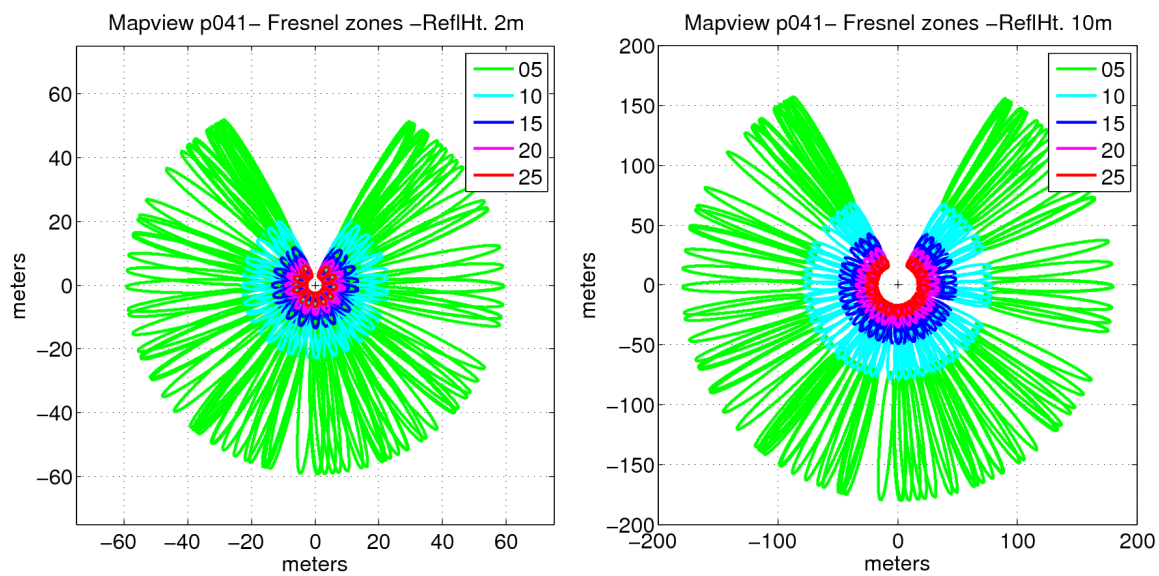


Figure 1. First Fresnel zones in mapview for GNSS site P041 near Boulder, Colorado. Elevation angles are defined by colors in the legend. Two values of H_R are used: 2 meters (left) and 10 meters (right).

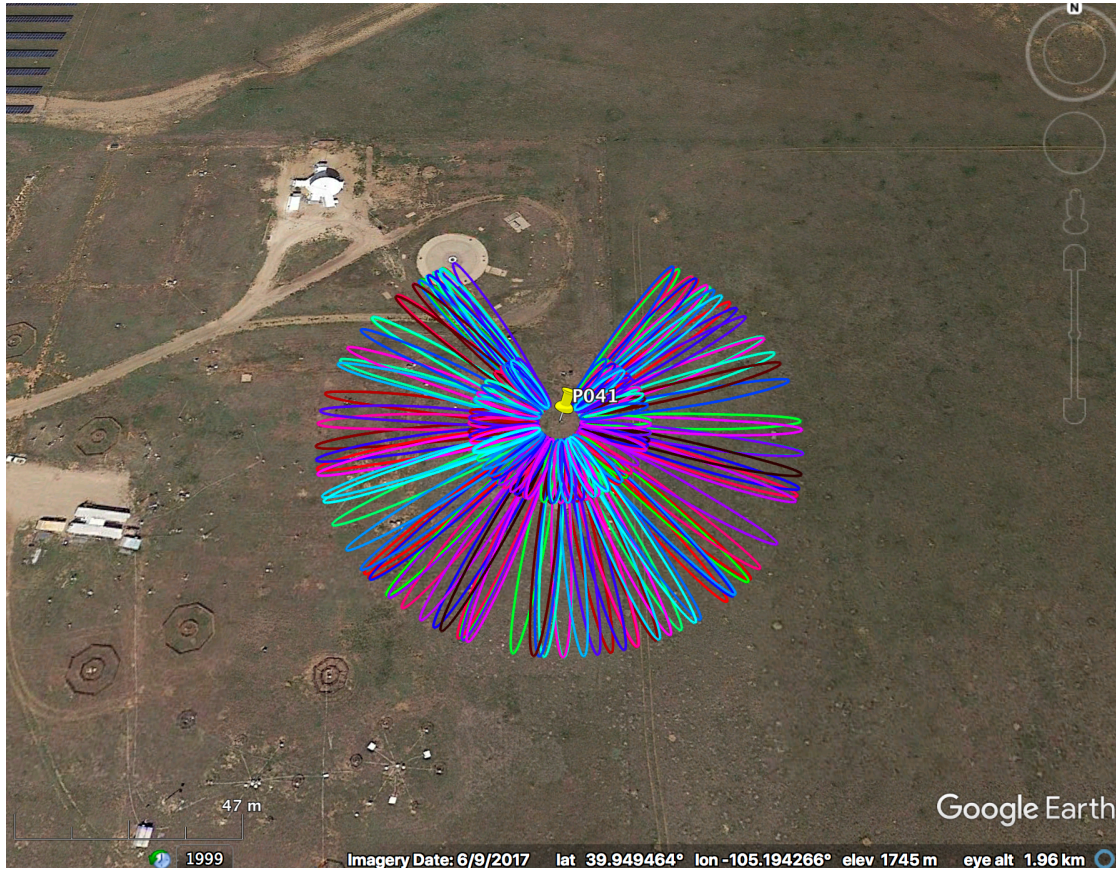


Figure 2. First Fresnel zones for GNSS site P041 for elevation angles of 5 and 10 degrees projected on a Google Earth image. An H_R value of 2 meter was used.

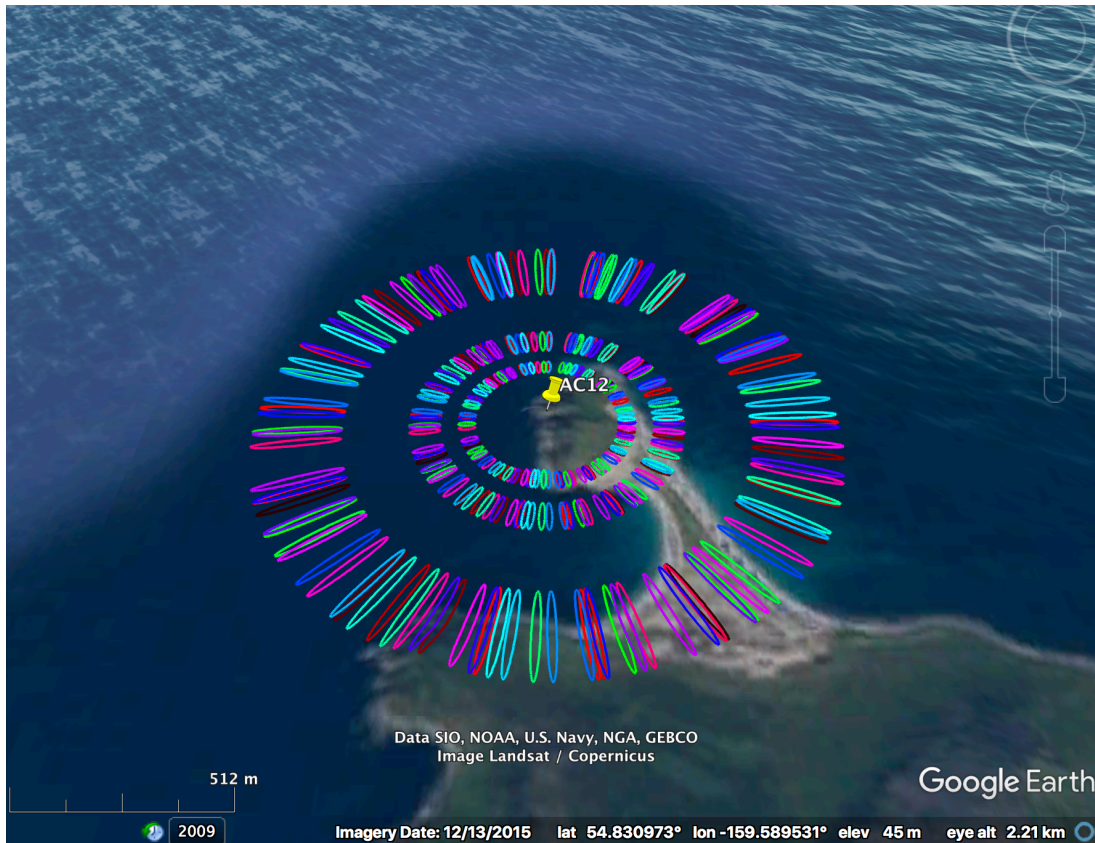


Figure 3. Screenshot of first Fresnel zones for GNSS site AC12 and elevation angles of 5, 7, and 10 degrees projected on a Google Earth image. An H_R value of 68 meters was used.

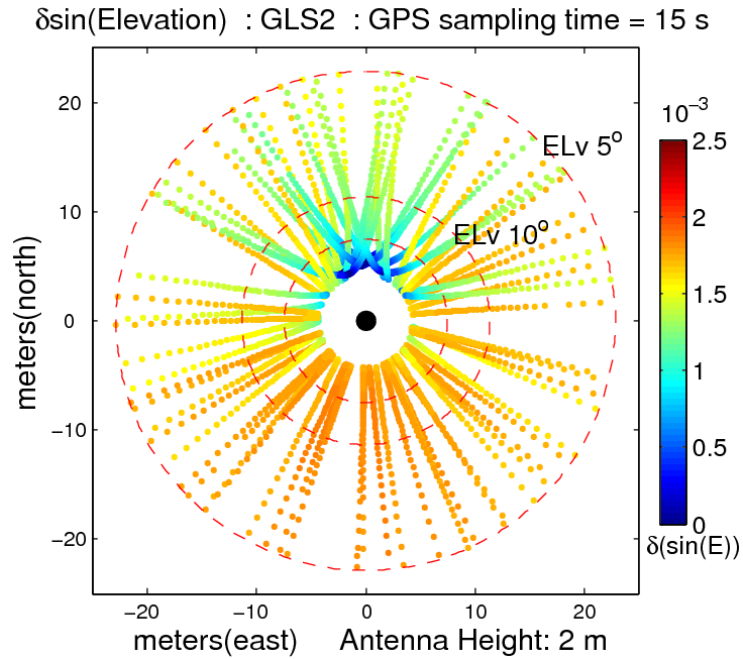


Figure 4. Interval between two $\sin(e(t))$ sampling variables for station GLS2 with a receiver sampling rate of 15 seconds. The markers are projected on the satellite ground track for a 2-meter antenna height. We only plot a marker every minute because the markers are very close for higher satellite elevation angles.

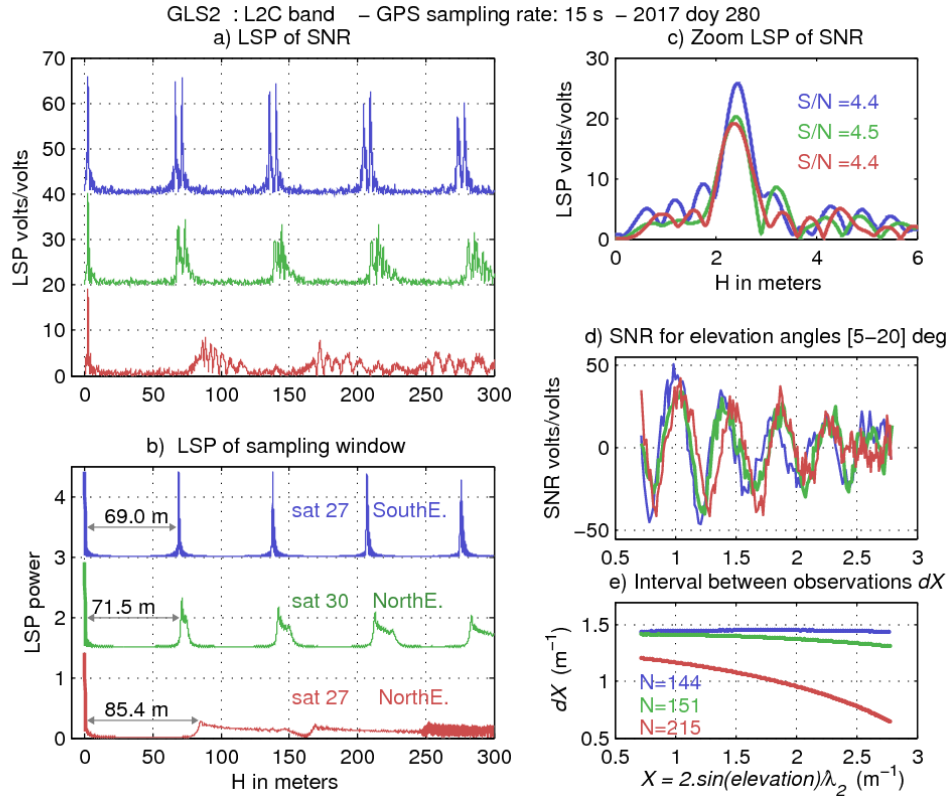


Figure 5. Effect of GNSS type survey window with uneven sampling on the LSP of SNR data. We show three survey windows for L2C data spanning the elevation range [5-20] from the GNSS station GLS2. The latter has a receiver sampling-rate of 15 seconds. Satellite 27's southeast track (blue) has nearly uniform samplings. Satellite 30's northeast track (green) has moderately uneven samplings. Satellite 27's northeast track (red) has the most uneven samplings found at this site. a) LSP of SNR data between 0 and 300 meters. b) LSP of sampling windows. c) Zoom of LSP of SNR data between 0 and 6 meters. d) SNR data with the same characteristics, as a function of the sampling variable $X(t)=2\sin(e(t))/\lambda_2$ in units of inverse meters. e) Interval between observations dX as a function of X . Note that in this figure we use X as the variable because it is this sampling variable which expresses the spectral frequencies directly in meters.

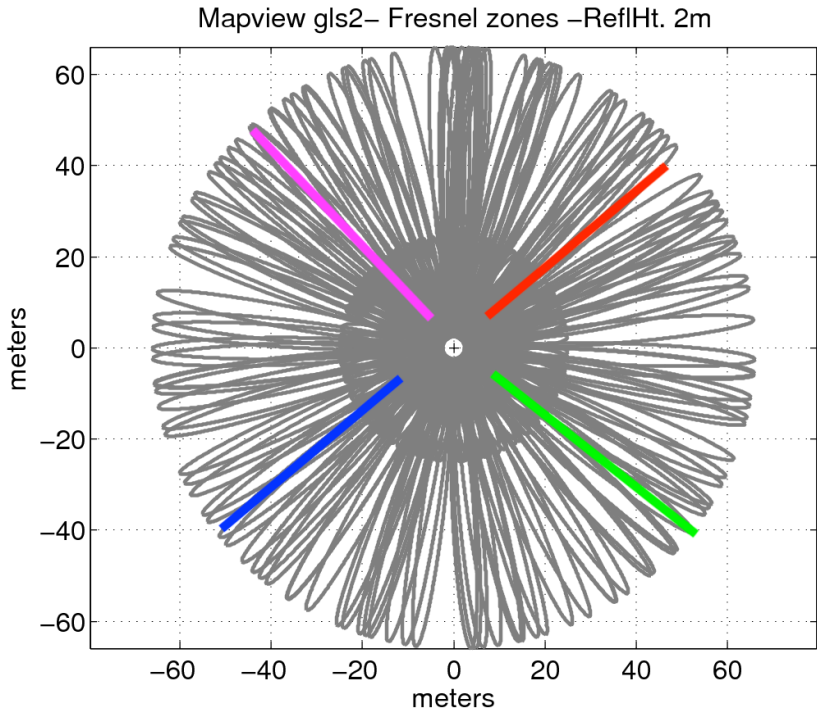


Figure 6. Mapview representation of the first Fresnel zones for elevation angles of 5,10,15, and 20 degrees (gray) for all GPS satellites at site GLS2 in Greenland (Larson et al 2015). The colors show the approximate azimuth of GPS satellite 30 that rises and sets twice at this site, once in each geographic quadrant. The cross at the coordinates 0,0 represents the GLS2 antenna.

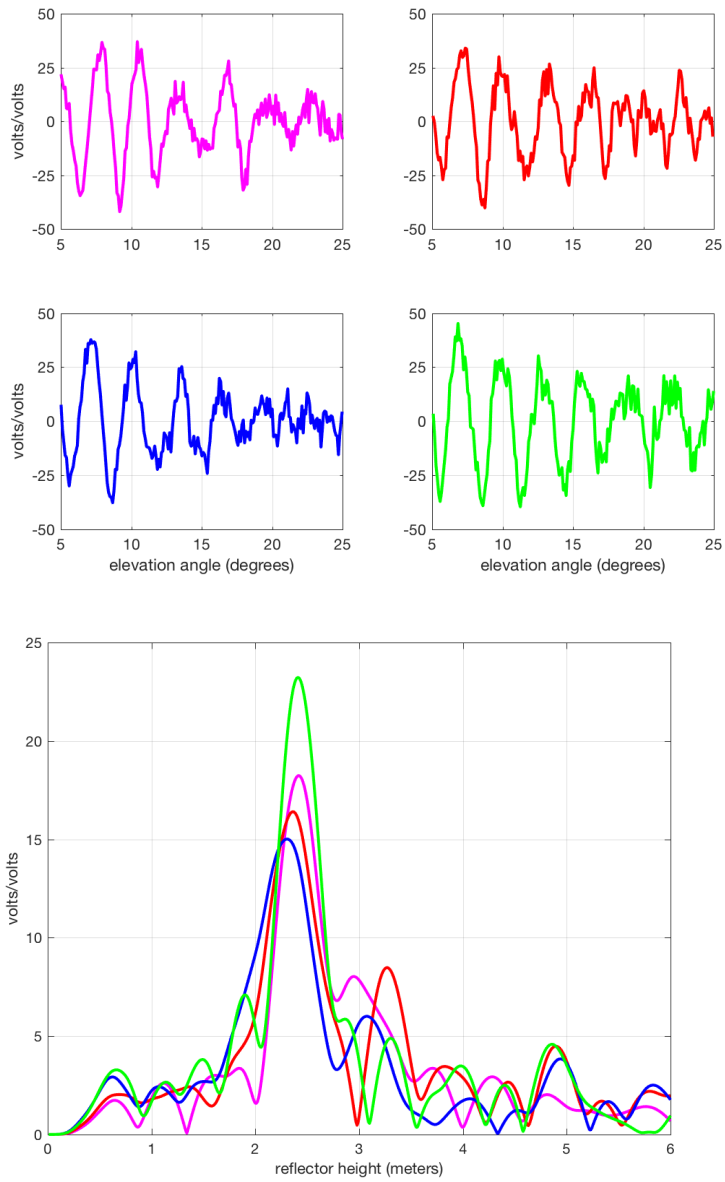


Figure 7. Top: L2C GPS SNR data for GNSS site GLS2 and satellite 30 on December 31, 2017. Quadrants are as shown in Figure 6; bottom: Lomb Scargle Periodograms for the SNR data shown above.

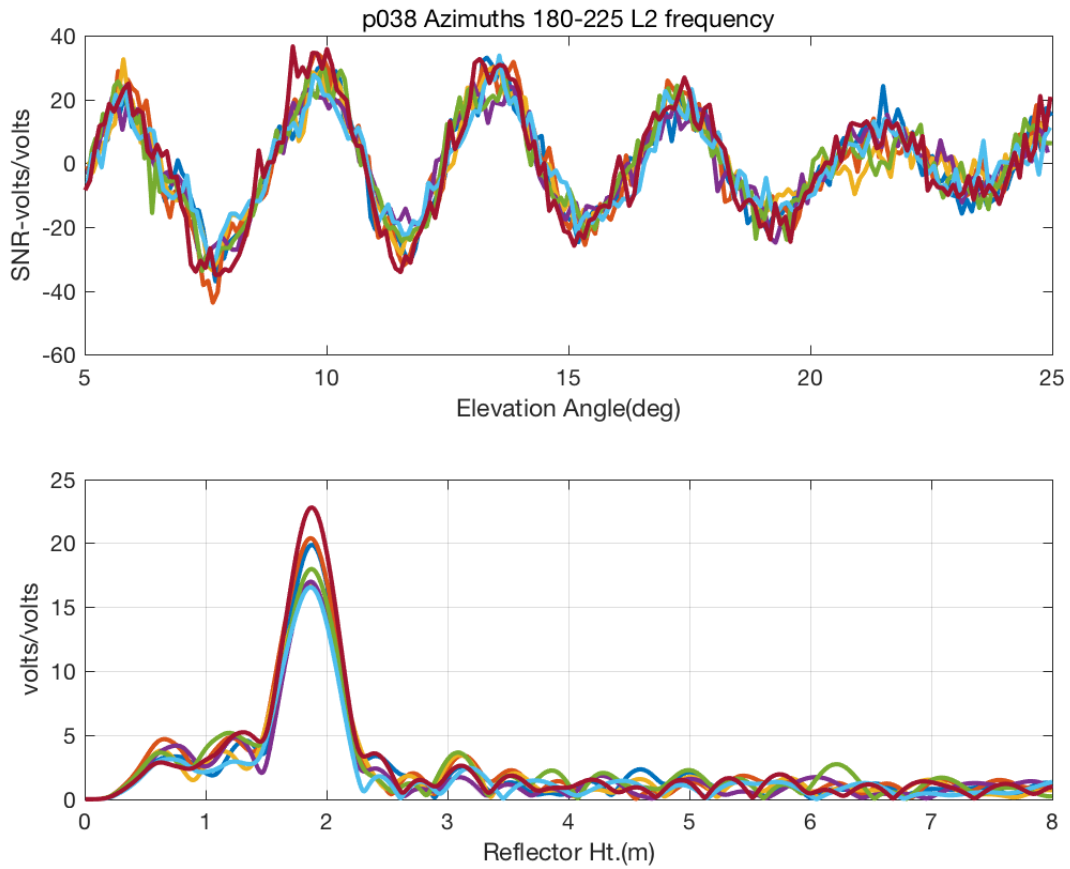


Figure 8. Top: L2C SNR data for GNSS station P038 on January 1, 2018 in an azimuth bin 180-225; bottom: Lomb Scargle Periodograms for data shown above.

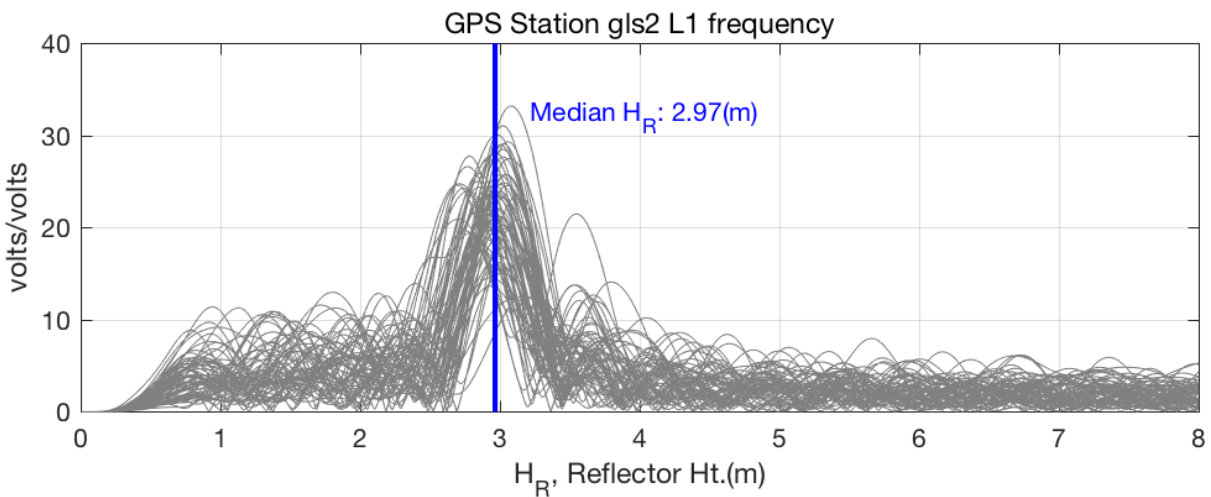


Figure 9. Lomb Scargle Periodograms for L1 SNR data from GNSS station GLS2 on May 24, 2013.